Auxiliary master equation approach to the Anderson-Holstein impurity problem out of equilibrium

Daniel Werner [1,*] Rok Žitko [2,3,†] and Enrico Arrigoni [1,‡]

[1]*Institute of Theoretical and Computational Physics, Graz University of Technology, 8010 Graz, Austria*
[2]*Jožef Stefan Institute, Jamova 39, SI-1000 Ljubljana, Slovenia*
[3]*Faculty of Mathematics and Physics, University of Ljubljana, Jadranska 19, SI-1000 Ljubljana, Slovenia*

We introduce a method based on the auxiliary master equation for solving the problem of an impurity with local electron-electron and electron-phonon interaction embedded between two conduction leads with a finite-bias voltage. The Anderson-Holstein Hamiltonian is transformed to a corresponding Lindblad equation with a reduced set of sites, providing an optimal approximation of the hybridization function. The problem is solved in the superfermion representation, using a configuration interaction for fermions and bosons. The phonon basis is shifted and rotated with the intention of permitting a low phonon basis cutoff, even in the strong-coupling regime. We benchmark this approach with the numerical renormalization group in equilibrium, finding excellent agreement. We observe, however, that the rotation brings no advantage beyond the bare shift. This is even more apparent out of equilibrium, where issues in convergence with respect to the size of the phononic Hilbert space occur only in the rotated basis. As an application of the method, we explore the evolution of the phononic peak in the differential conductance spectra with changing phonon frequency.

I. INTRODUCTION

Molecular electronics is the endeavor of using single molecules as components in ultraminiaturized circuits, making use of their particular electronic and vibration properties [1–14]. Nonequilibrium properties of single molecules can be probed by embedding molecules in gaps between electrodes [15], in mechanically controlled break junctions [16], as well as using scanning tunneling spectroscopy [17,18]. In these setups it is possible to apply bias voltages that are large compared to characteristic energy scales of the problem, such as interlevel spacing, phonon frequency, and electron-electron repulsion. Spectroscopic measurements are, however, difficult to interpret, because the strongly interacting problems are difficult to solve reliably and accurately out of equilibrium. A number of theoretical tools have been developed in the past [19–31], but no method has emerged yet as the ultimate solution applicable to all parameter domains. The key effective parameters are the dimensionless coupling strength $\lambda = g/\omega_b$, the adiabatic parameter $\alpha = \omega_b/U$ that relates electronic and vibrational energies, as well as the ratio Γ/U that quantifies the impurity hybridization; here g is the electron-phonon (e-ph) coupling constant, ω_b the phonon frequency, U the electron-electron repulsion, and Γ the hybridization strength. The parameters λ and α allow one to define the limiting cases of weak and strong e-ph coupling ($\lambda \ll 1$ vs $\lambda \gg 1$), as well as the adiabatic and the antiadiabatic limits ($\alpha \ll 1$ vs $\alpha \gg 1$);

the regime away from the various limits is known as the intermediate (crossover) regime.

In Ref. [19] the electron-vibron coupling in the Kondo regime is investigated using the Schrieffer-Wolff transformation, where the parameter regime is restricted to weak coupling. The semiclassical approach presented in Ref. [20] goes beyond the mean-field decoupling of electrons and phonons, and coincides well with quantum Monte Carlo results for sufficiently high temperatures. However, due to its nature it misses quantum processes like tunneling, so in the current implementation lower temperatures may not be reached. For a nonequilibrium equation-of-motion approach, implemented in Ref. [21], the authors point out that results obtained by their method in the Kondo regime are questionable beyond the low-bias regime. Reference [22] applies the dynamical mean-field theory to the Holstein-Hubbard model by solving the resulting the Anderson-Holstein impurity problem using quantum Monte Carlo; good results are obtained, but only in equilibrium. The authors of Ref. [23] use the numerical renormalization group (NRG) to obtain equilibrium spectral functions. To obtain the tunneling current, however, they use perturbation theory, which is restricted to the strong-coupling regime. In Ref. [24] the noncrossing approximation is implemented, which allows exploration of the Kondo regime at finite voltage; however, the electron-vibron coupling is restricted to small values. This approach is also used in Ref. [25], where the authors explore the effect of electron-vibron coupling in the Kondo regime for large Coulomb repulsion. An implementation of the functional renormalization group is shown in Ref. [26] (see also [32]), where good results are obtained in and out of equilibrium; however, the authors point out that their results are questionable for large electron interaction strength U out of

*daniel.werner96@posteo.at
†rok.zitko@ijs.si
‡arrigoni@tugraz.at

equilibrium. The nonequilibrium dual-boson approach shown in Ref. [27] appears quite similar to the approach presented in this work, with two main differences. First, they have a smaller bath, which they compensate by taking into account the difference between the physical and the auxiliary bath perturbatively. Second, they consider a phononic bath, which we do not. The authors obtain good results, but it appears to us that our method reproduces the Kondo peak more precisely; this can be observed from the coincidence of our self-energy results with the ones obtained by the NRG. Reference [28] discusses the hierarchical quantum master equation (HQME) approach in the context of electron-vibron coupling. This approach allows for numerically exact results but is restricted to moderate to high temperatures. One should mention, however, Ref. [29], where the HQME approach is extended for the pure electronic Anderson model, and accurate results for small temperatures are shown. Hierarchical equations of motion, Ref. [30], can handle non-Markovian system-bath interaction, but it may be difficult to keep truncation errors small. The NRG has been extended to the nonequilibrium steady-state case [31], but the proper description of thermal leads is technically demanding and requires combining several numerical methods to handle different energy scales (i.e., the NRG alone is not sufficient); this approach has not yet been applied to the Anderson-Holstein Hamiltonian.

In this work we present the auxiliary master equation approach for the Anderson-Holstein impurity problem [33–38]. Considering the above discussion, the method presented here complements the existing methods by bridging between different values of parameters, from weak to strong hybridization as well as interactions, and, importantly, by allowing temperatures below the Kondo scale to be reached for moderate values of the interaction. This Hamiltonian is the minimal description of a molecule with a single low-energy orbital with effective on-site electron-electron repulsion and with the coupling between the on-site charge and the displacement of a local vibration mode, embedded between two metallic conduction leads. The goal is to solve this problem in the regime of sizable electron-electron (e-e) and electron-phonon (e-ph) coupling for large bias voltages and to calculate the differential conductance, which is the main experimentally measurable quantity that provides information on the excitations in the system.

The paper is structured as follows. In Sec. II we start by discussing the basic idea of the auxiliary master equation approach (AMEA). We continue by briefly reviewing our implementation of configuration interaction (CI) for the electrons in Sec. II E 1 and discuss in more detail the CI treatment of phonons in Sec. II E 2. In Sec. III we first elaborate on the choice of method parameters. Then we benchmark the differential conductance against the numerical renormalization group in equilibrium in Sec. III B and show differential conductance results out of equilibrium in Sec. III C.

II. MODEL AND METHOD

A. Nonequilibrium Green's functions

We use the Keldysh formalism [39–44]. The time contour from $t \to -\infty$ to $t \to \infty$ and back again leads to a 2×2 matrix structure for including all time combinations, i.e., both
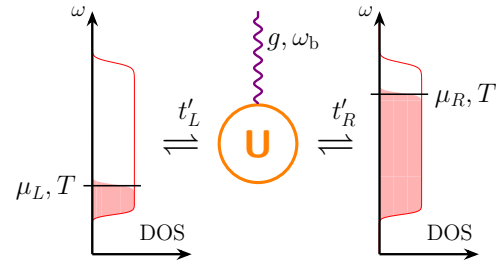

FIG. 1. Schematic representation of the system. Two leads at different chemical potentials are connected to an impurity with a Hubbard interaction U and a coupling to a Holstein phonon.

times on the upper contour, one above, and one below, etc. Since we are only interested in the steady state, we can take advantage of time translation invariance and fix one time argument of the Green's functions to zero. This allows us to work directly in the frequency domain instead of the time domain. The general form of a Green's function is then

$$\underline{G}(\omega) = \begin{pmatrix} G^{R}(\omega) & G^{K}(\omega) \\ 0 & G^{A}(\omega) \end{pmatrix}, \tag{1}$$

where $G^{A} = (G^{R})^{\dagger}$. Throughout this paper, underlined quantities represent a 2×2 structure in Keldysh space. In equilibrium, G^{K} can be determined from G^{R} via the fluctuation-dissipation theorem as

$$G^{K}(\omega) = F(\omega) 2i \text{Im}[G^{R}(\omega)], \tag{2}$$

with

$$F(\omega) = \begin{cases} \coth \frac{\beta\omega}{2} & \text{for bosons,} \\ \tanh \frac{\beta\omega}{2} & \text{for fermions.} \end{cases} \tag{3}$$

B. Physical impurity model

The physical setup consists of an impurity, two electronic reservoirs, and one local phonon mode, as depicted in Fig. 1. The respective Hamiltonian may be split up as

$$H = H_{\text{imp}} + H_{\text{bath}} + H_{\text{coup}}. \tag{4}$$

H_{imp} is the Hamiltonian of the impurity,

$$\varepsilon_{\text{imp}} \sum_{\sigma} d_{\sigma}^{\dagger} d_{\sigma} + U n_{d\uparrow} n_{d\downarrow} + \sum_{\sigma} g d_{\sigma}^{\dagger} d_{\sigma}(b + b^{\dagger}) + \omega_{\text{b}} b^{\dagger} b, \tag{5}$$

with Hubbard interaction U, on-site energy ε_{imp}, the creation (annihilation) operator $d_{\sigma}^{\dagger}$ (d_{σ}) of a fermion at the impurity site with spin σ, the creation (annihilation) operator $b^{\dagger}$ (b) of a boson, the fermionic particle number operator $n_{d\sigma}$, electron-phonon interaction strength g, and phonon frequency ω_{b}. The leads are described by

$$H_{\text{bath}} = \sum_{k\lambda\sigma} \varepsilon_{\lambda k} a_{\lambda k \sigma}^{\dagger} a_{\lambda k \sigma}, \tag{6}$$

with dispersion $\varepsilon_{\lambda k}$ and creation (annihilation) operator $a_{\lambda k \sigma}^{\dagger}$ ($a_{\lambda k \sigma}$) of a fermion in the left and right lead, $\lambda \in \{L, R\}$, labeled by momentum k. The coupling between the impurity

and the bath is given by

$$H_{\mathrm{coup}} = \frac{1}{\sqrt{N_k}} \sum_{k\lambda\sigma} t'_\lambda (a^\dagger_{\lambda k\sigma} d_\sigma + d^\dagger_\sigma a_{\lambda k\sigma}), \qquad (7)$$

where t'_λ is the coupling strength between the leads and the impurity, and $N_k \to \infty$ is the number of k points. Whenever not mentioned otherwise, we have $t'_L = t'_R$.

Alternatively, the environment may be described in terms of Green's functions by defining the retarded hybridization function [45]

$$\underline{\Delta}^R_{\mathrm{phys}}(\omega) = \sum_\lambda t'^2_\lambda \underline{g}^R_\lambda(\omega), \qquad (8)$$

where $\underline{g}^R_\lambda(\omega)$ are the retarded Green's functions of the decoupled leads. (The subscript ph here stands for "physical" in order to distinguish this hybridization function from the auxiliary function to be defined in the next section.) To fully define the problem, one needs to specify the band properties. We chose a flat density of states smoothed around the edges so that

$$-\mathrm{Im}\big[g^R_\lambda(\omega)\big] = \frac{\pi}{2D} \rho_{\mathrm{FD}}(\omega - D, T_{\mathrm{fict}}) \rho_{\mathrm{FD}}(-\omega - D, T_{\mathrm{fict}}), \qquad (9)$$

where ρ_{FD} is the Fermi-Dirac distribution, T_{fict} a fictitious temperature, and D the half bandwidth. The smoothing is introduced to avoid a sharp change that would reduce the quality of reproducing the environment within AMEA; T_{fict} merely quantifies the degree of smoothing. We take our energy unit E_0 such that $D = 10E_0$. Then we set $T_{\mathrm{fict}} = 0.5E_0$ throughout this paper. In Figs. 4–6(a) and 6(c) we have $-\mathrm{Im}[\Delta^R_{\mathrm{phys}}(\omega = 0)]/E_0 = 1$, in Figs. 8 and 6(b) and 6(d) we have $-\mathrm{Im}[\Delta^R_{\mathrm{phys}}(\omega = 0)]/E_0 = 0.49$, and in Fig. 7 we have $-\mathrm{Im}[\Delta^R_{\mathrm{phys}}(\omega = 0)]/E_0 = 0.64$.

Since the uncoupled leads themselves are in equilibrium, the Keldysh part of their Green's function can be calculated using the fluctuation-dissipation theorem, Eqs. (2) and (3). If not stated otherwise, the chemical potentials of the right and left reservoir are given as $\mu_R = -\mu_L = \phi/2$, i.e., $\phi = eV$ describes the voltage drop across the impurity.

C. Auxiliary impurity model

Since the physical model is defined in an infinitely large Hilbert space, one has to find a way of approximating it for numerical computations on a reduced set of sites. The basic idea of the AMEA is to set the parameters of the Lindblad equation so as to reproduce the physical hybridization function [46].

The Lindblad equation is given as

$$\begin{aligned}
\frac{\mathrm{d}\rho(t)}{\mathrm{d}t} &= \hat{L}\rho \\
&= -i[H_{\mathrm{aux}}, \rho] + \sum_{ij\sigma} \Gamma^{(1)}_{ij}\left(c_{j\sigma}\rho c^\dagger_{i\sigma} - \frac{1}{2}\{c^\dagger_{i\sigma} c_{j\sigma}, \rho\}\right) \\
&\quad + \sum_{ij} \Gamma^{(2)}_{ij}\left(c^\dagger_{i\sigma}\rho c_{j\sigma} - \frac{1}{2}\{c_{j\sigma} c^\dagger_{i\sigma}, \rho\}\right),
\end{aligned} \qquad (10)$$

where $c^\dagger_{i\sigma}$ ($c_{i\sigma}$) is the fermionic creation (annihilation) operator, ρ is the density matrix, $\Gamma^{(1)}_{ij}$ and $\Gamma^{(2)}_{ij}$ describe the dissipative contributions, and H_{aux} is the unitary part, given as

$$\begin{aligned}
H_{\mathrm{aux}} &= \sum_{\substack{i,j:\langle ij\rangle \wedge (i,j)\neq(0,0)}}^{\sigma} E_{ij} c^\dagger_{i\sigma} c_{j\sigma} + U n_{f\uparrow} n_{f\downarrow} \\
&\quad + \sum_\sigma g c^\dagger_{f\sigma} c_{f\sigma}(b + b^\dagger) + \omega_b b^\dagger b \\
&= \underbrace{\sum_{\substack{i,j:\langle ij\rangle \wedge i,j\neq 0}}^{\sigma} E_{ij} c^\dagger_{i\sigma} c_{j\sigma}}_{H_{\mathrm{aux\,env}}} + \underbrace{\sum_{i\in\{-1,1\},\sigma} E_{fi} c^\dagger_{i\sigma} c_{f\sigma} + \mathrm{H.c.}}_{H_{\mathrm{aux\,coup}}} \\
&\quad + \left.\begin{matrix} \sum_\sigma \varepsilon_{\mathrm{imp}} c^\dagger_{f\sigma} c_{f\sigma} + g c^\dagger_{f\sigma} c_{f\sigma}(b + b^\dagger) \\ + U n_{f\uparrow} n_{f\downarrow} + \omega_b b^\dagger b \end{matrix}\right\} H_{\mathrm{aux\,imp}} .
\end{aligned} \qquad (11)$$

We define $f := 0$, which is the impurity site, and the indices i and j can assume integer values from $-N_B/2$ to $N_B/2$, where N_B is the number of bath sites. In this paper we only consider cases in which $N_B = 6$. This number of bath sites already allows for a large number of parameters, which can be seen when considering that the $\mathbf{\Gamma}$ matrices are only restricted to be positive semidefinite. In other words, the number of parameters used to fit $\underline{\Delta}_{\mathrm{aux}}$ to $\underline{\Delta}_{\mathrm{phys}}$ increases quadratically in N_B. In Ref. [46] it is furthermore explicitly shown that $N_B = 6$ suffices to reproduce a flat density of states accurately.

The part of H_{aux} denoted as $H_{\mathrm{aux\,imp}}$ is equivalent to H_{imp}. $H_{\mathrm{aux\,coup}}$ describes the coupling between the auxiliary reservoirs and the impurity, i.e., its parameters are set by t'_λ. All the other contributions appearing in Eq. (11) are determined in a fitting procedure, which we will discuss in the following.

The auxiliary hybridization function $\underline{\Delta}_{\mathrm{aux}}$ is defined through

$$\begin{aligned}
\underline{G}_{0ff} &= (\underline{g}_0 - \underline{\Delta}_{\mathrm{aux}})^{-1} \rightarrow \\
\Delta^R_{\mathrm{aux}}(\omega) &= 1/g^R_{0,ff}(\omega) - 1/G^R_{0,ff}(\omega), \\
\Delta^K_{\mathrm{aux}}(\omega) &= G^K_{0,ff}(\omega)/\big|G^R_{0,ff}(\omega)\big|^2,
\end{aligned} \qquad (12)$$

where $\underline{G}_{0ff}$ is given [46] by

$$\begin{aligned}
\mathbf{G}^R_0(\omega) &= [\omega - \mathbf{E} + i(\mathbf{\Gamma}^{(1)} + \mathbf{\Gamma}^{(2)})]^{-1}, \\
\mathbf{G}^K_0(\omega) &= 2i\mathbf{G}^R_0(\omega)(\mathbf{\Gamma}^{(2)} - \mathbf{\Gamma}^{(1)})\mathbf{G}^A_0(\omega)
\end{aligned} \qquad (13)$$

and $g^R_{0,ff}$ as

$$g^R_{0,ff}(\omega) = (\omega - \varepsilon_{\mathrm{imp}})^{-1}. \qquad (14)$$

A note on notation: Bold quantities indicate the $(N_B + 1) \times (N_B + 1)$ structure in the space of auxiliary levels, lowercase

g indicates the decoupled setup, uppercase G contains the coupling, and the index 0 indicates the noninteracting case.

Given the physical hybridization function Δ_{ph}, one defines a cost function

$$\chi(\boldsymbol{E}, \boldsymbol{\Gamma}^{(1)}, \boldsymbol{\Gamma}^{(2)}) = \sum_{\alpha \in \{R, K\}} \int_{-\infty}^{\infty} d\omega \, W^{\alpha}(\omega)$$
$$\times \operatorname{Im}\left[\Delta_{\mathrm{phys}}^{\alpha}(\omega) - \Delta_{\mathrm{aux}}^{\alpha}(\omega; \boldsymbol{E}, \boldsymbol{\Gamma}^{(1)}, \boldsymbol{\Gamma}^{(2)})\right]^2,$$

which must be minimized to obtain the parameters leading to the optimal approximation of the physical hybridization function.

In this paper we set the weight function to $W^{\alpha}(\omega) = \Theta(|\omega - \omega_{\max}|)$, with $\omega_{\max}/E_0 = 15$. This range suffices to capture the hybridization function appropriately, since our flat density of states ranges from $\omega/E_0 = -10$ to 10 and decays exponentially outside this region. A more detailed discussion about the fitting procedure can be found in Ref. [46].

D. Superfermion representation

For computational reasons, one may transform the Lindblad equation into the superfermion representation [47]. In this form the Lindbladian becomes a matrix and the density matrix a vector. In this section we will briefly sketch the basic ideas of this procedure roughly following Ref. [47], see also Refs. [48,49].

We introduce the left vacuum [50] defined as

$$|I\rangle = \sum_{\{m_{\mathrm{el}}, m_{\mathrm{ph}}\}} \underbrace{(|m_{\mathrm{el}}\rangle \otimes |m_{\mathrm{ph}}\rangle)}_{\text{normal space}} \otimes \underbrace{(|\tilde{m}_{\mathrm{el}}\rangle \otimes |\tilde{m}_{\mathrm{ph}}\rangle)}_{\text{tilde space}}, \quad (15)$$

where m_{el} and m_{ph} run over all states in the respective Hilbert spaces. Here we doubled the Hilbert space by introducing the "tilde" space.

Then we apply the density matrix on the left vacuum:

$$\rho \to |\rho\rangle = (\rho \otimes \tilde{\mathbb{1}})|I\rangle$$
$$= \left(\sum_{mn} \rho_{mn} |m\rangle \langle n| \otimes \tilde{\mathbb{1}}\right) \left(\sum_{j} |j\rangle \otimes |\tilde{j}\rangle\right)$$
$$= \sum_{mnj} \rho_{mn}(|m\rangle \langle n|j\rangle) \otimes |\tilde{j}\rangle = \sum_{mn} \rho_{mn} |m\rangle \otimes |\tilde{n}\rangle. \quad (16)$$

This yields a vector in the doubled Hilbert space that contains all information of the density matrix. As the next step, the Lindbladian must also be transformed accordingly. The aim is to replace all density matrices appearing in L with $|\rho\rangle$. Therefore we calculate $L|I\rangle$, and whenever $|I\rangle$ is next to ρ we can use Eq. (16). To achieve this one uses the tilde-conjugation rules, given as

$$c_j^{\dagger} |I\rangle = -i\tilde{c}_j |I\rangle,$$
$$c_j |I\rangle = -i\tilde{c}_j^{\dagger} |I\rangle,$$
$$b^{\dagger} |I\rangle = \tilde{b} |I\rangle,$$
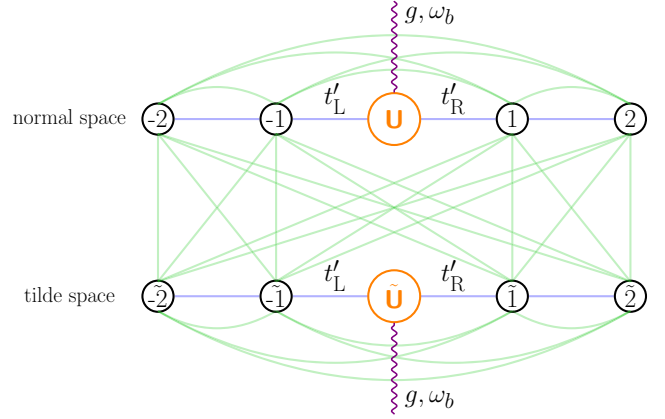$$b |I\rangle = \tilde{b}^{\dagger} |I\rangle, \quad (17)$$

FIG. 2. Schematic representation of the auxiliary system.

since the creation and annihilation operators, once transferred into the tilde space, commute with the density matrix [51] and anticommute (fermionic) or commute (bosonic) with the normal-space operators. The Lindbladian then takes the form

$$iL = \sum_{\sigma} \boldsymbol{c}_{\sigma}^{\dagger} \boldsymbol{h} \boldsymbol{c}_{\sigma} - 2\operatorname{Tr}(\boldsymbol{E} + i\boldsymbol{\Lambda})$$
$$+ U(n_{f\uparrow} n_{f\downarrow} - \tilde{n}_{f\uparrow} \tilde{n}_{f\downarrow})$$
$$\underbrace{+ \omega_{\mathrm{b}}(b^{\dagger}b - \tilde{b}^{\dagger}\tilde{b}) + g[c_{f\sigma}^{\dagger} c_{f\sigma}(b + b^{\dagger}) - \tilde{c}_{f\sigma}^{\dagger} \tilde{c}_{f\sigma}(\tilde{b} + \tilde{b}^{\dagger})]}_{iL_{\mathrm{eph}}},$$
$$(18)$$

with the matrix

$$\boldsymbol{h} = \begin{pmatrix} \boldsymbol{E} + i\boldsymbol{\Omega} & 2\boldsymbol{\Gamma}^{(2)} \\ -2\boldsymbol{\Gamma}^{(1)} & \boldsymbol{E} - i\boldsymbol{\Omega} \end{pmatrix}, \quad (19)$$

where $\boldsymbol{c}_{\sigma}^{\dagger} = (c_{-N_B/2, \sigma}^{\dagger}, \ldots, c_{N_B/2, \sigma}^{\dagger}, \tilde{c}_{-N_B/2, \sigma}, \ldots, \tilde{c}_{N_B/2,\sigma})$, $\boldsymbol{\Omega} = \boldsymbol{\Gamma}^{(2)} - \boldsymbol{\Gamma}^{(1)}$, and $\boldsymbol{\Lambda} = \boldsymbol{\Gamma}^{(2)} + \boldsymbol{\Gamma}^{(1)}$. As defined in Sec. II C, the impurity site is indexed $f := 0$. Figure 2 shows the Lindblad setup in its superfermion form [52], where the blue lines represent the unitary contributions ($\boldsymbol{E}$) and the green ones the dissipative contributions ($\boldsymbol{\Gamma}^{(1/2)}$). Furthermore, since the Lindbladian in Eq. (18) is not a superoperator anymore, it does not carry the double hat. This also allows us to easily distinguish between superoperators and operators in superfermion space.

As can be deduced from Eq. (18), normal and tilde fermionic particles are always created and annihilated simultaneously and therefore their difference is conserved, i.e.,

$$N_{\sigma} - \tilde{N}_{\sigma} = \sum_{i} (c_{i\sigma}^{\dagger} c_{i\sigma} - \tilde{c}_{i\sigma}^{\dagger} \tilde{c}_{i\sigma}). \quad (20)$$

This is valid for both spins separately, since angular momentum is also conserved.

Since the left vacuum is always a left eigenstate of the Lindbladian with eigenvalue zero, it lies in the subspace $N_{\sigma} - \tilde{N}_{\sigma} = 0$. This can be observed from Eq. (15), since all fermionic states have by definition the same number of normal and tilde electrons. Since the corresponding right eigenvector is the steady state, it is restricted to the same subspace.

The fermionic Green's functions can be expressed in the Lehmann representation. For positive times (+) the greater (>) and lesser (<) component are given as

$$
\begin{aligned}
G_{ij}^{>+}(\omega) &= \sum_k \langle I | c_i | k\mathrm{R} \rangle \langle k\mathrm{L} | c_j^\dagger | \rho_\infty \rangle \frac{1}{\omega - \mathrm{i} L_k}, \\
G_{ij}^{<+}(\omega) &= \sum_k \langle I | c_j^\dagger | k\mathrm{R} \rangle \langle k\mathrm{L} | c_i | \rho_\infty \rangle \frac{1}{\omega + \mathrm{i} L_k},
\end{aligned}
\tag{21}
$$

where $\langle k\mathrm{L} |$ and $| k\mathrm{R} \rangle$ are the left and right eigenvectors of the Lindbladian and L_k the corresponding eigenvalues. From this all other fermionic Green's functions of interest, as well as the self-energy (Σ), can be obtained:

$$
\begin{aligned}
G_{ij}^{\gtrless -}(\omega) &= -[G_{ji}^{\gtrless +}(\omega)]^*, \\
G_{ij}^{\mathrm{R}}(\omega) &= G_{ij}^{>+} - G_{ij}^{<-}, \\
G_{ij}^{\mathrm{K}}(\omega) &= G_{ij}^{>+} + G_{ij}^{<+} - G_{ij}^{>-} - G_{ij}^{<-}, \\
\Sigma^{\mathrm{R}}(\omega) &= 1/G_0^{\mathrm{R}}(\omega) - 1/G^{\mathrm{R}}(\omega), \\
\Sigma^{\mathrm{K}}(\omega) &= -G_0^{\mathrm{K}}(\omega)/\big|G_0^{\mathrm{R}}(\omega)\big|^2 + G^{\mathrm{K}}(\omega)/\big|G^{\mathrm{R}}(\omega)\big|^2.
\end{aligned}
\tag{22}
$$

For bosonic Green's functions there exist similar expressions as Eqs. (21) and (22). Computationally, we calculate the steady state using the biconjugate gradient method, and the Green's function using the bi-Lanczos scheme [53]. The basis used to express L is obtained as described in the next section.

E. Configuration interaction

The most straightforward basis choice for L is in terms of $c/c^\dagger$ and $b/b^\dagger$ operators. Then one can perform the calculation using the full many-body Lindbladian using a cutoff in the number of included phonons. The resulting matrix grows exponentially in the system size N_B. Therefore we rotate the bosonic and fermionic single-particle operators with the aim of cutting off the fermionic states in a controlled way and obtaining a reduced cutoff in the bosonic states. This is discussed in the following sections, where we roughly follow Ref. [54].

1. Electrons

The treatment of electrons in the AMEA using CI is explained in detail in Ref. [55]. Here we will only give a brief overview of the main steps. We start by defining

$$
\begin{aligned}
E_{ij\sigma} &= E_{ij} + U \langle n_{f\bar\sigma} \rangle \delta_{if}\delta_{jf} - 2\frac{g^2 \langle n_f \rangle}{\omega_{\mathrm{b}}}, \\
\boldsymbol{h}_\sigma &= \begin{pmatrix} \boldsymbol{E}_\sigma + \mathrm{i}\boldsymbol{\Omega} & 2\boldsymbol{\Gamma}^{(2)} \\ -2\boldsymbol{\Gamma}^{(1)} & \boldsymbol{E}_\sigma - \mathrm{i}\boldsymbol{\Omega} \end{pmatrix},
\end{aligned}
\tag{23}
$$

where $\langle n_{f\sigma} \rangle = \langle I | c_{f\sigma}^\dagger c_{f\sigma} | \rho_\infty \rangle$ and $\langle n_f \rangle = \langle n_{f\uparrow} \rangle + \langle n_{f\downarrow} \rangle$. Here $\boldsymbol{E}_\sigma$ (and thereby $\boldsymbol{h}_\sigma$) takes into account the electron-electron and electron-phonon (the origin of the phononic term will become clear in the following, see Sec. II E 2) interaction on a mean-field level.

The matrix $\boldsymbol{E}_\sigma$ is in principle the same for both spins, since there is no magnetic term in the Lindbladian. We showed in Ref. [55] that choosing a spin-dependent (magnetized) Hartree-Fock term reduces the error originating from the

basis cutoff we introduce within CI. The respective mean-field (Hartree-Fock) Lindbladian reads

$$
\mathrm{i} L_{0\mathrm{el}} = \sum_\sigma \boldsymbol{c}_\sigma^\dagger \boldsymbol{h}_\sigma \boldsymbol{c}_\sigma - \underbrace{\sum_\sigma \mathrm{Tr}(\boldsymbol{E}_\sigma + \mathrm{i}\boldsymbol{\Lambda})}_{\eta}.
\tag{24}
$$

In our previous paper we fixed $\langle n_{f\uparrow} \rangle = 0.3$ and $\langle n_{f\downarrow} \rangle = 0.7$ to introduce an artificial magnetization. The exact values for $\langle n_{f\sigma} \rangle$ do not have a strong influence on the shape of the impurity Green's function, as long as it is far enough from $\langle n_{f\uparrow} \rangle = \langle n_{f\downarrow} \rangle$ but not too far (roughly in the range 0.6–0.9). Since not all the results we show here are particle-hole symmetric, we compute the total Hartree-Fock electron occupation self-consistently using Eq. (24) and introduce a magnetization as $\langle n_{f\uparrow} \rangle = 0.3 \langle n_f \rangle$, $\langle n_{f\downarrow} \rangle = 0.7 \langle n_f \rangle$.

The non-Hermitian matrix $\boldsymbol{h}_\sigma$ can be diagonalized straightforwardly as

$$
\boldsymbol{\varepsilon}_\sigma = \boldsymbol{V}_\sigma^{-1} \boldsymbol{h}_\sigma \boldsymbol{V}_\sigma,
\tag{25}
$$

where $\boldsymbol{V}_\sigma$ ($\boldsymbol{V}_\sigma^{-1}$) are the right (left) eigenvectors of $\boldsymbol{h}_\sigma$, and $\boldsymbol{\varepsilon}_\sigma$ its eigenvalues. In this basis the Hartree-Fock Lindbladian reads

$$
\mathrm{i} L_{0\mathrm{el}} = \sum_\sigma \bar{\boldsymbol{\xi}}_\sigma \boldsymbol{\varepsilon}_\sigma \boldsymbol{\xi}_\sigma + \eta.
\tag{26}
$$

The new operators are defined as $\bar{\boldsymbol{\xi}}_\sigma = \boldsymbol{c}_\sigma^\dagger \boldsymbol{V}_\sigma$ and $\boldsymbol{\xi}_\sigma = \boldsymbol{V}_\sigma^{-1} \boldsymbol{c}_\sigma$, which obey fermionic anticommutation relations. However, the creation and annihilation operators are not Hermitian conjugates of each other, i.e., $(\xi)^\dagger \neq \bar{\xi}$.

The steady state of the noninteracting Lindbladian $L_{0\mathrm{el}}$ can be found by identifying which operators annihilate it. In other words, we must have

$$
\begin{aligned}
\xi_{i\sigma} | \rho_{\infty 0\mathrm{el}} \rangle &= 0 \quad \text{for } \mathrm{Im}(\varepsilon_{i\sigma}) < 0, \\
\bar{\xi}_{i\sigma} | \rho_{\infty 0\mathrm{el}} \rangle &= 0 \quad \text{for } \mathrm{Im}(\varepsilon_{i\sigma}) > 0,
\end{aligned}
\tag{27}
$$

because anything else would imply a divergent state, as becomes apparent when considering

$$
\mathrm{e}^{L_0 t} \xi_{i\sigma} | \rho_{\infty 0\mathrm{el}} \rangle = \mathrm{e}^{L_0 t} \xi_{i\sigma} \mathrm{e}^{-L_0 t} | \rho_{\infty 0\mathrm{el}} \rangle = \mathrm{e}^{\mathrm{i}\varepsilon_{i\sigma} t} \xi_{i\sigma} | \rho_{\infty 0\mathrm{el}} \rangle.
\tag{28}
$$

For computational reasons we furthermore perform a particle-hole transformation

$$
\begin{aligned}
\boldsymbol{P} &= \bar{\boldsymbol{D}}\boldsymbol{\xi} + \bar{\boldsymbol{\xi}}\boldsymbol{D}, \\
\bar{\boldsymbol{P}} &= \boldsymbol{D}\boldsymbol{\xi} + \bar{\boldsymbol{\xi}}\bar{\boldsymbol{D}},
\end{aligned}
\tag{29}
$$

with components

$$
\begin{aligned}
D_{ij} &= \delta_{ij}\Theta[\mathrm{Im}(\varepsilon_i)], \\
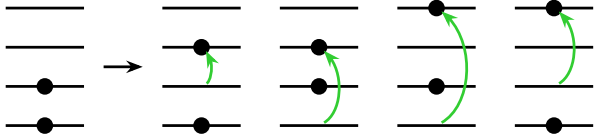\bar{D}_{ij} &= 1 - D_{ij}.
\end{aligned}
\tag{30}
$$

From this we get $| \rho_{0\mathrm{el}} \rangle = | 0 \rangle$.

Starting from the Hartree-Fock steady state as a reference state, we can create a subspace of excited states by applying operator pairs,

$$
\bar{\xi}_{i\sigma} \xi_{j\sigma} | \rho_{\infty 0\mathrm{el}} \rangle,
\tag{31}
$$

which is equivalent to

$$
\bar{P}_{i\sigma} \bar{P}_{j\sigma} | 0 \rangle,
\tag{32}
$$

FIG. 3. Illustration of Eq. (31) for a small Hilbert space. The reference state, in our case the steady state of Eq. (24), is shown on the left-hand site. On its right-hand site all the states one obtains from a single excitation are depicted.

with i and j taking all values resulting in nonvanishing states, which obeys the conservation rules, namely, $N_\sigma - \tilde{N}_\sigma = c_\sigma$, where c_σ is a spin-dependent constant. For the steady state we have $c_\downarrow = c_\uparrow = 0$ and for the Green's functions $c_{\downarrow/\uparrow} = 0$ and $c_{\uparrow/\downarrow} = \pm 1$. The state in Eq. (31) corresponds to a single "particle-hole" excitation and can be graphically interpreted as depicted in Fig. 3 (shown in the ξ basis). By applying more such pairs in sequence, one obtains higher excitations. In this paper we always use a basis created by up to three particle-hole excitations (referred to in the literature as CISDT).

Eventually Eq. (18) is transformed into the P basis such that the fermionic contributions to the matrix elements in the many-body Lindblad matrix can be calculated in this subspace.

2. Phonons

When including phonons, the Hilbert space becomes in principle infinite so that one has to introduce a cutoff in the maximum phonon number. The larger the cutoff, the better the approximation for observables, but at the cost of higher memory usage and longer computation times. By choosing an advantageous single-particle basis, the number of bosonic particles can be kept low while still obtaining accurate results.

One starts by introducing an offset to the bosonic operators, which corresponds to the NECI* shift introduced in Ref. [54], whose treatment we roughly follow below. This shifts the number of phonons in the new vacuum to the amount corresponding to the mean-field electron occupation, i.e., without taking into account the effect of electronic fluctuations:

$$b \to b - \frac{g\langle n_f \rangle}{\omega_b}, \quad b^\dagger \to b^\dagger - \frac{g\langle n_f \rangle}{\omega_b},$$
$$\tilde{b} \to \tilde{b} - \frac{g\langle n_f \rangle}{\omega_b}, \quad \tilde{b}^\dagger \to \tilde{b}^\dagger - \frac{g\langle n_f \rangle}{\omega_b}. \quad (33)$$

The corresponding Lindblad term in the superfermion representation then reads

$$iL_{\text{eph}} = \sum_\sigma \frac{2g^2 \langle n_f \rangle}{\omega_b}(\tilde{c}_{f\sigma}^\dagger \tilde{c}_{f\sigma} - c_{f\sigma}^\dagger c_{f\sigma}) + \omega_b(b^\dagger b - \tilde{b}^\dagger \tilde{b})$$
$$+ g(b + b^\dagger)(c_{f\sigma}^\dagger c_{f\sigma} - \langle n_f \rangle)$$
$$+ g(\tilde{b} + \tilde{b}^\dagger)(\langle n_f \rangle - \tilde{c}_{f\sigma}^\dagger \tilde{c}_{f\sigma}). \quad (34)$$

In the next step one "rotates" the phononic basis, i.e., one introduces a linear transformation between the "tilde" and "non-tilde" phononic creation and annihilation operator, as first introduced in Ref. [54]. This transformation is obtained

by the exact solution of an auxiliary Lindblad equation acting on the isolated phonon level:

$$\hat{L}_{\text{0ph}}\rho = \alpha_+ \left(b^\dagger \rho b - \tfrac{1}{2}\{\rho, bb^\dagger\} \right) + \alpha_- \left(b\rho b^\dagger - \tfrac{1}{2}\{\rho, b^\dagger b\} \right)$$
$$+ i[bb^\dagger \omega_b, \rho]. \quad (35)$$

This equation can be obtained exactly by eliminating the "fermionic reservoir" from the isolated phonon level within the weak-coupling ($g/\omega_b \ll 1$) regime with the Born-Markov-Secular approximation [56,57]. In this case the ratio $\frac{\alpha_-}{\alpha_+}$ can be written in terms a suitable fermionic density-density correlation function, and in the equilibrium case can be inferred from the relation

$$\text{Tr}\{b^\dagger b \rho_{\infty 0\text{ph}}\} = \frac{\alpha_+}{\alpha_- - \alpha_+} \to \exp(\beta\omega_b) = \frac{\alpha_-}{\alpha_+}. \quad (36)$$

With this we rewrite the impurity Lindbladian L_{imp} as

$$L_{\text{imp}} = L_{\text{int}} + L_{\text{onsite}} + L_{\text{HF}}$$
$$L_{\text{HF}} = L_{\text{0el}} + L_{\text{0ph}}$$
$$iL_{\text{int}} = Un_\uparrow n_\downarrow + iL_{\text{eph}} - iL_{\text{HF}} \quad (37)$$
$$iL_{\text{onsite}} = \varepsilon_{\text{imp}} + \sum_\sigma \frac{2g^2 \langle n_f \rangle}{\omega_b}(\tilde{c}_{f\sigma}^\dagger \tilde{c}_{f\sigma} - c_{f\sigma}^\dagger c_{f\sigma}),$$

with L_{0ph} being the superfermion version of $\hat{L}_{\text{0ph}}$ given as

$$L_{\text{0ph}} = \alpha_+ \left(b^\dagger \tilde{b} - \frac{1}{2}\tilde{b}\tilde{b}^\dagger - \frac{1}{2}b^\dagger b \right)$$
$$+ \alpha_- \left(\tilde{b}b - \frac{1}{2}\tilde{b}\tilde{b}^\dagger - \frac{1}{2}b^\dagger b \right) - i\omega_b(b^\dagger b - \tilde{b}\tilde{b}^\dagger)$$
$$+ \frac{\alpha_- - \alpha_+}{2} - i\omega_b. \quad (38)$$

L_{0el} contains the mean-field on-site energies felt by the electrons due to the e-e and e-ph coupling, and L_{0ph} considers the thermalization effect the electrons have on the phonons. L_{int} then contains corrections beyond the mean-field level felt by the electrons, as well as corrections to the thermalization effect the electrons have on the phonons.

In the case of the electrons, we used the matrices diagonalizing L_{0el} to transform the electronic single-particle operators. For the phonons we proceed in a similar way, where we start by rewriting L_{0ph}:

$$L_{\text{0ph}} = \boldsymbol{b}^\dagger \boldsymbol{h}_{\text{0ph}} \boldsymbol{b} + \eta_{\text{0ph}}$$
$$= \underbrace{\boldsymbol{b}^\dagger \boldsymbol{S} \boldsymbol{U} \boldsymbol{S}}_{\bar{\boldsymbol{\varphi}}} \underbrace{\boldsymbol{S} \boldsymbol{U}^{-1} \boldsymbol{S} \boldsymbol{h}_{\text{0ph}} \boldsymbol{U}}_{\varepsilon} \underbrace{\boldsymbol{U}^{-1} \boldsymbol{b}}_{\boldsymbol{\varphi}} + \eta_{\text{0ph}}, \quad (39)$$

where

$$\boldsymbol{b} = (b^\dagger \quad \tilde{b}),$$
$$\eta_{\text{0ph}} = \frac{\alpha_- - \alpha_+}{2} - i\omega_b,$$
$$\boldsymbol{h}_{\text{0ph}} = \begin{pmatrix} -\frac{1}{2}(\alpha_+ + \alpha_-) - i\omega_b & \alpha_+ \\ \alpha_- & -\frac{1}{2}(\alpha_+ + \alpha_-) + i\omega_b \end{pmatrix},$$
$$\boldsymbol{S} = [\boldsymbol{b}, \boldsymbol{b}^\dagger] = \begin{pmatrix} 1 & 0 \\ 0 & -1 \end{pmatrix}, \quad (40)$$

and U are the right eigenvectors of $\boldsymbol{Sh}_{0\mathrm{ph}}$. For convenience we define

$$\psi_1 := \phi_1, \bar{\psi}_1 := \bar{\phi}_1, \psi_2 := \bar{\phi}_2, \bar{\psi}_2 := \phi_2 \qquad (41)$$

such that

$$[\psi, \bar{\psi}] = \mathbb{1}. \qquad (42)$$

In the ψ basis the Lindbladian $L_{0\mathrm{ph}}$ is diagonal; therefore the steady state is given by a single Fock state, which is simultaneously the vacuum in this basis ($|\rho_{\infty 0\mathrm{ph}}\rangle = |00\rangle$) [58]. This state contains the thermalizing effect the electrons have on the phonons, making it a good choice for a reference state

[59] to build the phononic basis from:

$$(\bar{\psi}_1)^n (\bar{\psi}_2)^m |0\rangle . \qquad (43)$$

We define the cutoff value for the number of included phonons per site as "$N_{\mathrm{ph,max}}$" (number of phonons), i.e., $0 \leqslant n, m \leqslant N_{\mathrm{ph,max}}$, with n, m integers. To transform Eq. (34) in the ψ basis we use

$$\mathbf{b} = \begin{pmatrix} \psi_1 + \frac{\alpha_+}{\alpha_-} \bar{\psi}_2 \\ \psi_1 + \bar{\psi}_2 \end{pmatrix}$$
$$\mathbf{b}^\dagger = \begin{pmatrix} \bar{\psi}_1 + \psi_2 & \frac{\alpha_+}{\alpha_-} \bar{\psi}_1 + \psi_2 \end{pmatrix} \frac{\alpha_-}{\alpha_- - \alpha_+}, \qquad (44)$$

which follows from Eqs. (39) and (41). With this L_{eph} in its final version reads

$$iL_{\mathrm{eph}} = \sum_\sigma 2 \frac{g^2 \langle n_f \rangle}{\omega_{\mathrm{b}}} (c_{f\sigma}^\dagger c_{f\sigma} - \tilde{c}_{f\sigma}^\dagger \tilde{c}_{f\sigma}) + g(c_{f\sigma}^\dagger c_{f\sigma} - \langle n_f \rangle) \left(\frac{\alpha_-}{\alpha_- - \alpha_+} (\bar{\Psi}_1 + \Psi_2) + \Psi_1 + \frac{\alpha_+}{\alpha_-} \bar{\Psi}_2 \right)$$
$$+ g(\langle n_f \rangle - \tilde{c}_{f\sigma}^\dagger \tilde{c}_{f\sigma}) \left(\Psi_1 + \bar{\Psi}_2 + \frac{1}{\alpha_- - \alpha_+} (\alpha_+ \bar{\Psi}_1 + \alpha_- \Psi_2) \right) + \omega_{\mathrm{b}} (\bar{\Psi}_2 \Psi_2 - \bar{\Psi}_1 \Psi_1). \qquad (45)$$

III. RESULTS

A. Method parameters

In equilibrium the parameters α_+ and α_- can be calculated straightforwardly from the temperature of the system. Only the ratio $\frac{\alpha_-}{\alpha_+}$ appears in equations; thus there is actually a single
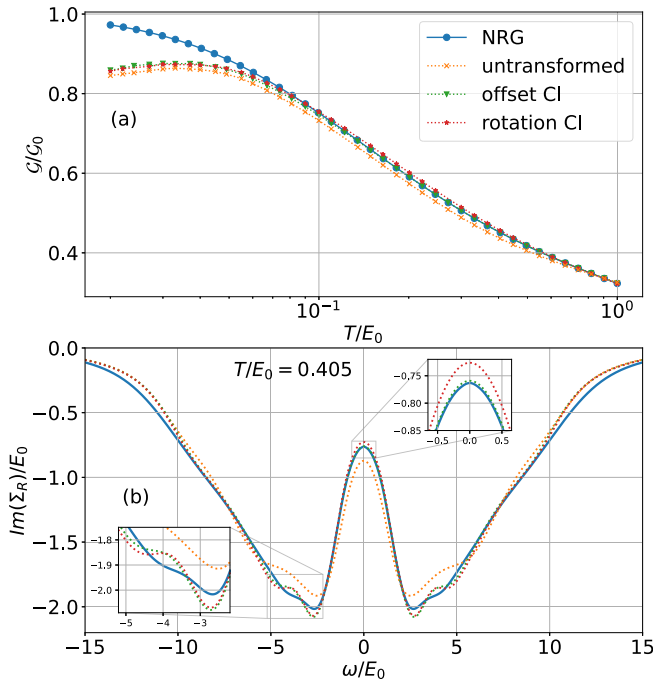

FIG. 4. (a) Zero-bias conductance as function of temperature and (b) self-energy $\mathrm{Im}(\Sigma_R)$ obtained with different transformations as explained in the text. The parameters are $U/E_0 = 6$, $g/E_0 = 1.3$, $\omega_{\mathrm{b}}/E_0 = 1.3$, $\varepsilon_{\mathrm{imp}} = -U/2 + 2g^2/\omega_{\mathrm{b}}$, $-\mathrm{Im}[\Delta_{\mathrm{phys}}^R(\omega = 0)]/E_0 = 1.0$, and $N_{\mathrm{ph,max}} = 5$.

free parameter that is fixed by β. Out of equilibrium we need to choose an effective temperature felt by the phonons, which is, however, not defined unambiguously. Two approaches were considered: (a) fitting the Fermi function $\rho_{\mathrm{FD}}(\omega - \mu, T)$ to the nonequilibrium distribution $\rho_{\mathrm{non\text{-}eq}}(\omega)$, and (b) enforcing $\rho_{\mathrm{FD}}(w = \omega_{\mathrm{b}}) = \rho_{\mathrm{non\text{-}eq}}(w = \omega_{\mathrm{b}})$. In both cases the effective temperature felt by the phonons is extracted. Comparing the results obtained from both procedures showed that fitting works better. Here we calculate the nonequilibrium distribution $\rho_{\mathrm{non\text{-}eq}}(\omega)$ from Eq. (24), i.e., for the mean-field case. This is computationally much less costly than performing an iterative many-body calculation to obtain this parameter.

All parameters that are purely an input to the simulation have been chosen such that the Kondo regime can be investigated in the presence of a Holstein phonon as a proof of concept.

B. Comparison with the NRG in equilibrium

As a benchmark of the approach presented in this work, we compare our results with the NRG in the equilibrium case, where the latter is known to be very accurate, especially in the low-energy regions.

First, we investigate how the transformation of the phononic basis introduced in Sec. II E 2 affects the accuracy of the calculation. More specifically, we compare the results obtained without any transformation, those with only the offset ("offset CI"), Eq. (33), and those with both the offset and the rotation ("rotation CI"), Eqs. (44) and (33). We plot the zero-bias conductance as a function of temperature, which provides insight into the effect of the transformations at low energies over a wide temperature range. While the differential conductance mainly probes the low-energy region, we address higher energies by evaluating $\mathrm{Im}[\Sigma_R(\omega)]$. From the Meir-Wingreen formula [60] one obtains the nonequilibrium

differential conductance $\mathcal{G}$ as

$$
\mathcal{G} = \int_{-\infty}^{\infty} \frac{d\omega}{\pi} \text{Im}[G^R(\omega, \phi)] \frac{\gamma_L(\omega)\gamma_R(\omega)}{\gamma_L(\omega) + \gamma_R(\omega)} \left(\frac{d\rho_{F,L}(\omega, \mu_L, T)}{d\phi} \right.
$$

$$
\left. - \frac{d\rho_{F,R}(\omega, \mu_R, T)}{d\phi} \right) + \int_{-\infty}^{\infty} \frac{d\omega}{\pi} \frac{d\text{Im}[G^R(\omega, \phi)]}{d\phi}
$$

$$
\times \frac{\gamma_L(\omega)\gamma_R(\omega)}{\gamma_L(\omega) + \gamma_R(\omega)} [(\rho_{F,L}(\omega, \mu_L, T) - \rho_{F,R}(\omega, \mu_R, T)]
$$

$$(46)$$

for the case of proportional coupling. Here $\gamma_\lambda(\omega) = -2|t_\lambda'^2|\text{Im}[g_\lambda^R(\omega)]$ are also referred to as the "lead self-energies." In the following we will always plot the ratio $\mathcal{G}/\mathcal{G}_0$. As $T \to 0$ the spectral function at zero frequency becomes independent of the interaction strength [61,62]. Therefore, the dc conductance always approaches $\mathcal{G} = \mathcal{G}_0$ for $T \to 0$, where $\mathcal{G}_0$ is the conductance quantum.

The numerical renormalization group (NRG) [63–65] is well known for capturing the equilibrium properties very accurately. Therefore, we use the results obtained from NRG Ljubljana [66] as a reference for the equilibrium case. The calculations have been performed using the discretization parameter $\Lambda = 2$, with twist averaging over four discretization grids, keeping up to 10 000 spin multiplets in truncation and using the broadening parameter $\alpha = 0.2$. The final spectral functions have been computed using the self-energy trick, using the full-density-matrix approach [67]. We keep up to 15 phonon states in the calculation.

Both the offset CI and the rotation CI results compare very well with NRG and perform significantly better than the results obtained without any transformation, as can be seen in the differential conductance results in Fig. 4(a). The parameters are chosen so that the system is in the Kondo regime ($U > \pi\Gamma$) with an intermediately strong e-ph coupling $\lambda \sim 1$. Considering a maximum allowed deviation of 3% with respect to the NRG, temperatures down to $T/E_0 = 0.05$ can be reached for the chosen $U/E_0 = 6$ with both CI transformations. The offset CI performs marginally better. At very low temperature, the CI results deviate from those obtained by the NRG because the occupation function at the Fermi energy becomes sharper, which is reflected in a sharper Keldysh part of the hybridization function, requiring more bath sites (i.e., parameters) in the auxiliary system to reproduce the physical system accurately than are available.

The self-energies of the offset and rotation CI are also almost on top of each other, see Fig. 4(b). They mostly coincide with the NRG self-energy, except close to the phononic feature, which is more pronounced for the CI methods. We have compared the self-energies at a temperature which is close to that obtained for nonequilibrium at $\phi = \omega_b$ using the procedure discussed in Sec. III A.

With increasing phonon cutoff, we expect convergence of all observables. Figure 5 shows that the convergence behavior of the offset CI at low energies is superior. In the self-energy both approaches have trouble reaching full convergence close to the phononic feature.

The drop in the conductance with increasing temperature, which may be described via the half-width at half maximum
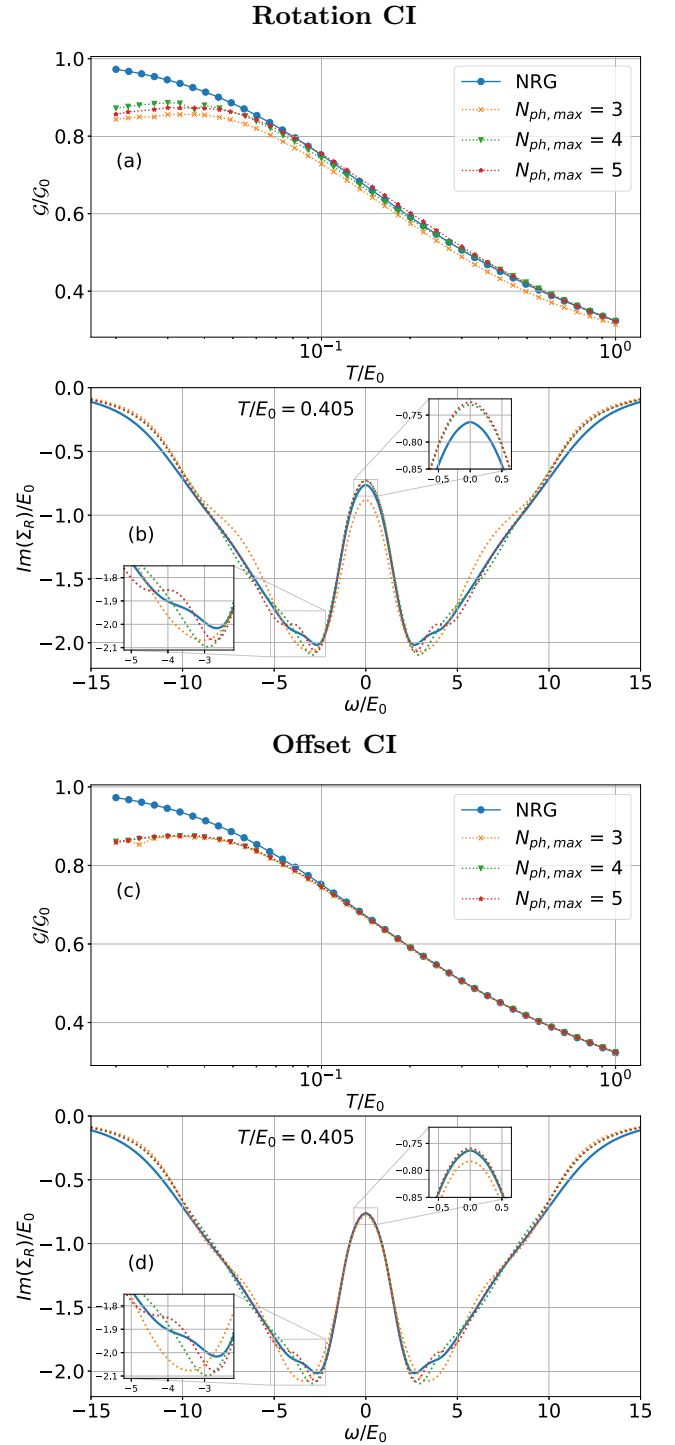

FIG. 5. Zero-bias conductance as function of temperature (a) and (c) and self-energy (b) and (d) for the CI calculation with different values of the phonon cutoff compared with NRG. Results are obtained with the rotation CI (a) and (b), offset CI (c) and (d). Parameters are as in Fig. 4.

(HWHM), is defined by the Kondo scale and is also a possible definition of the Kondo temperature (T_K). This definition of T_K was first introduced in Ref. [68], where an empirical formula is presented and used to fit the NRG zero-bias conductance [69], fulfilling $\mathcal{G}(T = T_K) = \mathcal{G}_0/2$. From Fig. 5 one can
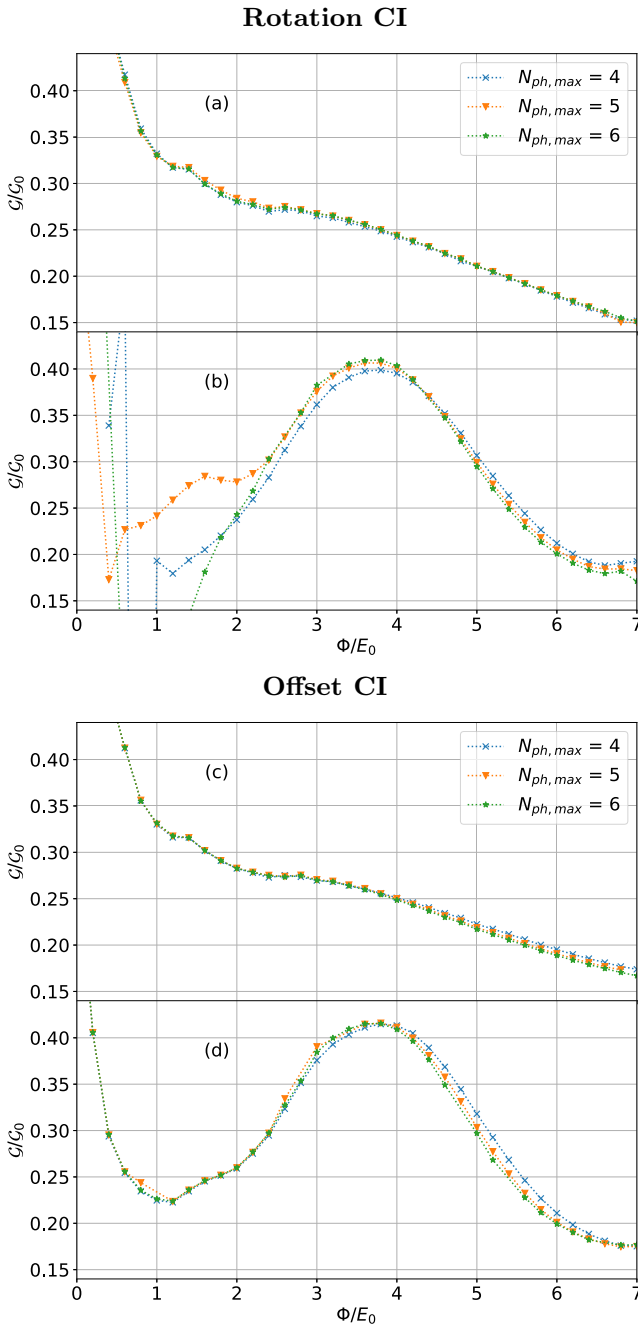
Rotation CI

Offset CI

FIG. 6. Nonequilibrium differential conductance as a function of voltage evaluated with different values of the phonon cutoff. Results are obtained with the rotation CI (a) and (b) or with the offset CI (c) and (d). (a, c) Results with strong lead coupling, $-\mathrm{Im}[\Delta^{\mathrm{R}}_{\mathrm{phys}}(\omega = 0)]/E_0 = 1.0$, (b, d) with weak lead coupling, $-\mathrm{Im}[\Delta^{\mathrm{R}}_{\mathrm{phys}}(\omega = 0)]/E_0 = 0.49$. Remaining parameters are $g/E_0 = 1.1$, $\omega_{\mathrm{b}} = 1.5$, $U/E_0 = 6$, $\varepsilon_{\mathrm{imp}} = -U/2 + 2g^2/\omega_{\mathrm{b}}$, $T/E_0 = 0.05$, $N_{\mathrm{ph,max}} = 5$. The rotation CI results do not converge for voltages close to zero and to the phonon frequency.

FIG. 7. Differential conductance variation with voltage for diverse $\gamma_{\mathrm{L}}/\gamma_{\mathrm{R}}$ ratios. Emphasis on asymmetry effects: in pronounced asymmetric scenarios, the differential conductance aligns closely with the equilibrium approximation, but as symmetry increases, nonequilibrium influences become evident. Key parameters: $\mu_{\mathrm{L}} = 0$, $\mu_{\mathrm{R}} = \phi$, and $-\mathrm{Im}[\Delta^{\mathrm{R}}_{\mathrm{phys}}(\omega = 0)]/E_0 = 0.64$. All other parameters are consistent with those in Fig. 6.

an effective value of $U \to U_{\mathrm{eff}} = U - 2g^2/\omega_{\mathrm{b}}$, and the lower the U value, the higher the Kondo temperature.

C. Nonequilibrium results

Having shown that in equilibrium the offset CI performs better than the rotation CI, especially at low energies, we now study if this is the case also in nonequilibrium. We consider the differential conductance as a function of applied voltage and start by investigating the convergence behavior as a function of the number of included phonons. We considered several values of the system-environment coupling (t'_λ), which we describe in terms of $-\mathrm{Im}[\Delta^{\mathrm{R}}_{\mathrm{phys}}(\omega = 0)] \propto t'^2_\lambda$ for easier notation. Decreasing $-\mathrm{Im}[\Delta^{\mathrm{R}}_{\mathrm{phys}}(\omega = 0)]$ is observed to give rise to a phononic feature at the phonon frequency.

Figure 6 shows that both transformations converge rapidly for stronger system-environment coupling. In the case of weaker coupling, which is when the phononic feature appears, the rotation CI fails at low voltages and does not converge at the phonon frequency. The offset CI, on the other hand, converges almost immediately over the full voltage range. Therefore, especially in nonequilibrium, the rotation does not prove to be advantageous. We expect that a (possibly partial) Lang-Firsov transformation [70–72] would bring improvements; this will be implemented in future work.

As in Fig. 5, showing a conductance drop as the temperature increases, a similar behavior can be observed in Fig. 6 as the voltage increases. Again the HWHM is set by the Kondo scale. For the parameters used here the respective voltages are $\Phi_{\mathrm{HWHM}}/E_0 = 0.58$ for the strong and $\Phi_{\mathrm{HWHM}}/E_0 = 0.39$ for the weak lead coupling. Comparing this with $\Phi_{\mathrm{HWHM}}/E_0 = 0.4$ for the strong and $\Phi_{\mathrm{HWHM}}/E_0 = 0.34$ for the weak lead

obtain $T_{\mathrm{K}}/E_0 = 0.3$. When comparing to the case of $g = 0$, one has for the otherwise same parameters $T_{\mathrm{K}}/E_0 = 0.2$. A lower temperature in the latter case is to be expected, since the electron-electron interaction is reduced by the phonons to

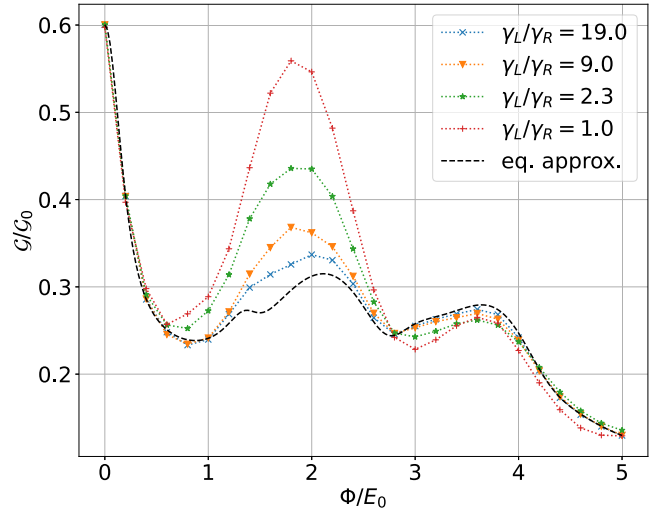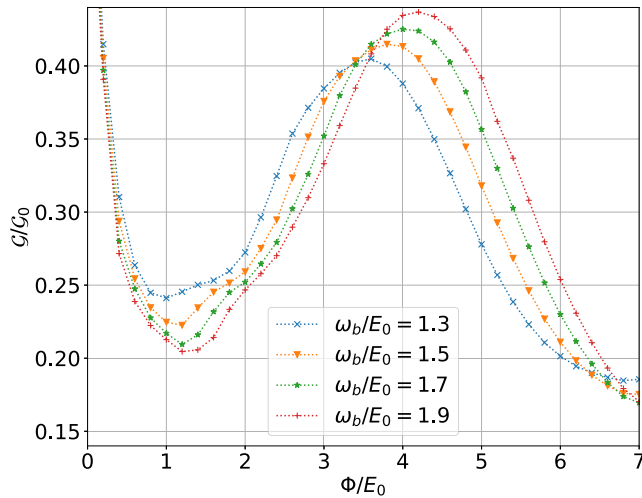FIG. 8. Variation in differential conductance with voltage for various ω_b values. As the phonon frequency is increased the phononic feature moves to the right, which is to be expected. The charge excitation also gets shifted, since the attraction felt by the electrons from the phonons decreases with increasing ω_b. The coupling to the environment is $-\mathrm{Im}[\Delta^R_{\mathrm{phys}}(\omega = 0)]/E_0 = 0.49$, and all other parameters are in line with Fig. 6.

coupling without phonons shows, as for the equilibrium case, that the effective reduction of U by the phonons increases the HWHM. The charge excitation can be observed to occur roughly at $\Phi/E_0 = 3.5$ [73].

We also investigated the crossover from very asymmetric lead coupling ($\frac{\gamma_L}{\gamma_R} \gg 1$) to the symmetric case, with γ_λ as introduced below Eq. (46). We use the offset CI here, since it proved to be superior to the rotation CI. For $\frac{\gamma_L}{\gamma_R} \gg 1$ the finite-bias differential conductance can be obtained using G^R from a zero-bias calculation [74]. Figure 7 shows the nonlinear differential conductance for a range of $\frac{\gamma_L}{\gamma_R}$ using the offset CI. The finite bias is applied by choosing $\mu_L = 0$ and $\mu_R = \phi$. For large asymmetry $\frac{\gamma_L}{\gamma_R} = 19$ we see that the differential conductance is very close to that obtained by the equilibrium approximation with $\frac{\gamma_L}{\gamma_R} \to \infty$. As we approach equal coupling of the leads, the nonequilibrium effects become apparent and the shape of the differential conductance curve changes significantly. The vibrational features are expected at $\Phi \sim \omega_b$, while the Coulomb peak is expected at $\Phi \sim U/2 = 3E_0$ [19,24,75].

Finally, we investigate the effect the phonon frequency has on the phononic feature in the fermionic spectrum. Again we use the offset CI. Figure 8 shows that the feature moves with ω_b, as one would expect, and that it is slowly "absorbed" in the charge excitation. The charge excitation itself is shifted to higher bias as the phonon frequency is increased. This comes again from the effective reduction of the Hubbard interaction by the phonons as discussed before.

In conclusion, we showed that the method discussed in Ref. [54] does not seem to provide any improvement of the accuracy of the CI calculation with respect to a simple shift in the phononic operators. This is the case especially in nonequilibrium, but also in equilibrium where the phonons have a well-defined temperature. Nevertheless, the equilibrium results presented coincide well with NRG, and the offset CI converges well in nonequilibrium as the phononic Hilbert space is increased.

IV. CONCLUSION

We have presented a solver for the Anderson-Holstein problem out of equilibrium. After mapping the Hamiltonian to an auxiliary impurity model in the form of a Lindblad equation and passing to the superfermion representation, we tackled the resulting problem using configuration interaction approach. In the electron sector we use a basis extending up to three particle-hole excitations, while in the phonon sector we attempted to optimize the basis using a shift and rotation, as introduced in Ref. [54]. The method was benchmarked against the numerical renormalization group results in equilibrium and then tested out of equilibrium. We find that in equilibrium the shift as well as the additional rotation allow for high accuracy using only a small phononic Hilbert space. However, the rotation, as discussed in Ref. [54], does not bring any advantage beyond purely shifting the operators and in some cases even introduces instabilities. Therefore, taking into account the effects of the fluctuating fermionic density on the phonon field does not seem to provide any advantage in the parameter region we have been considering. This becomes even more apparent in nonequilibrium, where the rotation leads to convergence problems in the number of phonons for some parameter regimes. Using the shifted operators, on the other hand, gives quickly converging results. We also use the offset CI to show the propagation of the phononic feature, as well as the charge excitation, due to changing phonon frequency. Our solver is thus capable of tackling the problem in the very demanding regime of large bias and strong interactions using only a shift in the phononic operators. Further improvements would consist of implementing the Lang-Firsov transformation. This could potentially lead to a capable solver for interpreting experimental bias spectra [76–81], unraveling the roles of electron-electron and electron-phonon interactions, and thereby increasing our understanding of the relation between the structure of molecules and their potentially useful electronic properties.

ACKNOWLEDGMENTS

[1] R. C. Jaklevic and J. Lambe, Molecular vibration spectra by electron tunneling, Phys. Rev. Lett. **17**, 1139 (1966).

[2] J. Lambe and R. C. Jaklevic, Molecular vibration spectra by inelastic electron tunneling, Phys. Rev. **165**, 821 (1968).

[3] A. Aviram and M. A. Ratner, Molecular rectifiers, Chem. Phys. Lett. **29**, 277 (1974).

[4] M. A. Reed, C. Zhou, C. J. Muller, T. P. Burgin, and J. M. Tour, Conductance of a molecular junction, Science **278**, 252 (1997).

[5] J. Chen, M. A. Reed, A. M. Rawlett, and J. M. Tour, Large on-off ratios and negative differential resistance in a molecular electronic device, Science **286**, 1550 (1999).

[6] A. Nitzan, Electron transmission through molecules and molecular interfaces, Annu. Rev. Phys. Chem. **52**, 681 (2001).

[7] Z. J. Donhauser, B. A. Mantooth, K. F. Kelly, L. A. Bumm, J. D. Monnell, J. J. Stapleton, D. W. Price, Jr., A. M. Rawlett, D. L. Allara, J. M. Tour, and P. S. Weiss, Conductance switching in single molecule through conformational changes, Science **292**, 2303 (2001).

[8] N. B. Zhitenev, H. Meng, and Z. Bao, Conductance of small molecular junctions, Phys. Rev. Lett. **88**, 226801 (2002).

[9] X. H. Qiu, G. V. Nazin, and W. Ho, Vibrationally resolved fluorescence excited with submolecular precision, Science **299**, 542 (2003).

[10] L. H. Yu, Z. K. Keane, J. W. Ciszek, L. Cheng, M. P. Stewart, J. M. Tour, and D. Natelson, Inelastic electron tunneling via molecular vibrations in single-molecule transistors, Phys. Rev. Lett. **93**, 266802 (2004).

[11] M. Galperin, M. A. Ratner, and A. Nitzan, Molecular transport junctions: Vibrational effects, J. Phys.: Condens. Matter **19**, 103201 (2007).

[12] N. A. Zimbovskaya and M. R. Pederson, Electron transport through molecular junctions, Phys. Rep. **509**, 1 (2011).

[13] H. Song, M. A. Reed, and T. Lee, Single molecule electronic devices, Adv. Mater. **23**, 1583 (2011).

[14] S. V. Aradhya and L. Venkataraman, Single-molecule junctions beyond electronic transport, Nat. Nanotechnol. **8**, 399 (2013).

[15] H. Park, J. Park, A. K. L. Lim, E. H. Anderson, A. P. Alivisatos, and P. L. McEuen, Nanomechanical oscillations in a single-C_{60} transistor, Nature (London) **407**, 57 (2000).

[16] N. Agraït, A. L. Yeyati, and J. M. van Ruitenbeek, Quantum properties of atomic-sized conductors, Phys. Rep. **377**, 81 (2003).

[17] B. C. Stipe, M. A. Rezaei, and W. Ho, Single-molecule vibrational spectroscopy and microscopy, Science **280**, 1732 (1998).

[18] F. Moresco, Manipulation of large molecules by low-temperature STM: Model systems for molecular electronics, Phys. Rep. **399**, 175 (2004).

[19] J. Paaske and K. Flensberg, Vibrational sidebands and the Kondo effect in molecular transistors, Phys. Rev. Lett. **94**, 176801 (2005).

[20] A. Picano, F. Grandi, P. Werner, and M. Eckstein, Stochastic semiclassical theory for nonequilibrium electron-phonon coupled systems, Phys. Rev. B **108**, 035115 (2023).

[21] M. Galperin, A. Nitzan, and M. A. Ratner, Inelastic effects in molecular junctions in the coulomb and Kondo regimes: Nonequilibrium equation-of-motion approach, Phys. Rev. B **76**, 035301 (2007).

[22] P. Werner and A. J. Millis, Efficient dynamical mean field simulation of the Holstein-Hubbard model, Phys. Rev. Lett. **99**, 146404 (2007).

[23] F. Eickhoff, E. Kolodzeiski, T. Esat, N. Fournier, C. Wagner, T. Deilmann, R. Temirov, M. Rohlfing, F. S. Tautz, and F. B. Anders, Inelastic electron tunneling spectroscopy for probing strongly correlated many-body systems by scanning tunneling microscopy, Phys. Rev. B **101**, 125405 (2020).

[24] P. Roura-Bas, L. Tosi, and A. A. Aligia, Nonequilibrium transport through magnetic vibrating molecules, Phys. Rev. B **87**, 195136 (2013).

[25] P. Roura-Bas, L. Tosi, and A. A. Aligia, Replicas of the Kondo peak due to electron-vibration interaction in molecular transport properties, Phys. Rev. B **93**, 115139 (2016).

[26] M. A. Laakso, D. M. Kennes, S. G. Jakobs, and V. Meden, Functional renormalization group study of the Anderson–Holstein model, New J. Phys. **16**, 023007 (2014).

[27] F. Chen, M. I. Katsnelson, and M. Galperin, Nonequilibrium dual-boson approach, Phys. Rev. B **101**, 235439 (2020).

[28] C. Schinabeck, A. Erpenbeck, R. Härtle, and M. Thoss, Hierarchical quantum master equation approach to electronic-vibrational coupling in nonequilibrium transport through nanosystems, Phys. Rev. B **94**, 201407(R) (2016).

[29] X. Dan, M. Xu, J. T. Stockburger, J. Ankerhold, and Q. Shi, Efficient low-temperature simulations for fermionic reservoirs with the hierarchical equations of motion method: Application to the Anderson impurity model, Phys. Rev. B **107**, 195429 (2023).

[30] Y. Tanimura, Numerically exact approach to open quantum dynamics: The hierarchical equations of motion (HEOM), J. Chem. Phys. **153**, 020901 (2020).

[31] F. Schwarz, I. Weymann, J. von Delft, and A. Weichselbaum, Nonequilibrium steady-state transport in quantum impurity models: A thermofield and quantum quench approach using matrix product states, Phys. Rev. Lett. **121**, 137702 (2018).

[32] A. Khedri, T. A. Costi, and V. Meden, Nonequilibrium thermoelectric transport through vibrating molecular quantum dots, Phys. Rev. B **98**, 195138 (2018).

[33] T. Holstein, Studied of polaron motion: Part I. The molecular-crystal model, Ann. Phys. **8**, 325 (1959).

[34] P. W. Anderson, Localized magnetic states in metals, Phys. Rev. **124**, 41 (1961).

[35] D. M. Newns, Self-consistent model of hydrogen chemisorption, Phys. Rev. **178**, 1123 (1969).

[36] G. S. Jeon, T.-H. Park, and H.-Y. Choi, Numerical renormalization-group study of the symmetric Anderson-Holstein model: Phonon and electron spectral functions, Phys. Rev. B **68**, 045106 (2003).

[37] A. C. Hewson and D. Meyer, Numerical renormalization group study of the Anderson-Holstein model, J. Phys.: Condens. Matter **14**, 427 (2002).

[38] P. S. Cornaglia, H. Ness, and D. R. Grempel, Many-body effects on the transport properties of single-molecule devices, Phys. Rev. Lett. **93**, 147201 (2004).

[39] J. Schwinger, Brownian motion of a quantum oscillator, J. Math. Phys. **2**, 407 (1961).

[40] L. P. Kadanoff and G. Baym, *Quantum Statistical Mechanics: Green's Function Methods in Equilibrium and Nonequilibrium Problems* (Addison-Wesley, Redwood City, CA, 1962).

[41] L. V. Keldysh, Diagram technique for nonequilibrium processes, Zh. Eksp. Teor. Fiz. **47**, 1515 (1964) [Sov. Phys. JETP **20**, 1018 (1965)].

[42] J. Rammer and H. Smith, Quantum field-theoretical methods in transport theory of metals, Rev. Mod. Phys. **58**, 323 (1986).

[43] H. Haug and A.-P. Jauho, *Quantum Kinetics in Transport and Optics of Semiconductors* (Springer, Heidelberg, 1998).

[44] M. Wagner, Expansions of nonequilibrium Green's functions, Phys. Rev. B **44**, 6104 (1991).

[45] E. N. Economou, *Green's Functions in Quantum Physics* (Springer, Heidelberg, 2006).

[46] A. Dorda, M. Sorantin, W. von der Linden, and E. Arrigoni, Optimized auxiliary representation of non-Markovian impurity problems by a Lindblad equation, New J. Phys. **19**, 063005 (2017).

[47] A. A. Dzhioev and D. S. Kosov, Super-fermion representation of quantum kinetic equations for the electron transport problem, J. Chem. Phys. **134**, 044121 (2011).

[48] A. Dorda, M. Nuss, W. von der Linden, and E. Arrigoni, Auxiliary master equation approach to non-equilibrium correlated impurities, Phys. Rev. B **89**, 165105 (2014).

[49] E. Arrigoni and A. Dorda, Master equations versus Keldysh Green's functions for correlated quantum systems out of equilibrium, in *Out-of-Equilibrium Physics of Correlated Electron Systems*, Springer Series in Solid-State Sciences Vol. 191, edited by R. Citro and F. Mancini (Springer International Publishing, Cham, Switzerland, 2018), Chap. 4, pp. 121–188.

[50] The left vacuum is always a left eigenstate with eigenvalue zero for arbitrary Lindbladians in superfermion representation. Furthermore, it is important when calculating observables, since it corresponds to taking the trace of the density matrix it is multiplied with.

[51] The density matrix has an even number of normal-space operators.

[52] Reference [46] shows that under usage of all available parameters, as is the case here, the geometry has no influence on the result. This justifies our choice here.

[53] C. Lanczos, An iteration method for the solution of the eigenvalue problem of linear differential and integral operators, J. Res. Natl. Bur. Stand. **45**, 255 (1950).

[54] A. A. Dzhioev and D. S. Kosov, Nonequilibrium configuration interaction method for transport in correlated quantum systems, J. Phys. A: Math. Theor. **47**, 095002 (2014).

[55] D. Werner, J. Lotze, and E. Arrigoni, Configuration interaction based nonequilibrium steady state impurity solver, Phys. Rev. B **107**, 075119 (2023).

[56] G. Schaller, *Open Quantum Systems Far from Equilibrium*, Lecture Notes in Physics (Springer, Heidelberg, 2014).

[57] H.-P. Breuer and F. Petruccione, *The Theory of Open Quantum Systems* (Oxford University Press, Oxford, England, 2009).

[58] Also, the left vacuum becomes the vacuum, i.e., $\langle I| = \langle 00|$, which it remains for arbitrary Lindbladians in this basis.

[59] Which is of importance if one restricts the Hilbert space, otherwise any arbitrary reference state would be equally good.

[60] Y. Meir and N. S. Wingreen, Landauer formula for the current through an interacting electron region, Phys. Rev. Lett. **68**, 2512 (1992).

[61] D. C. Langreth, Friedel sum rule for Anderson's model of localized impurity states, Phys. Rev. **150**, 516 (1966).

[62] J. S. Langer and V. Ambegaokar, Friedel sum rule for a system of interacting electrons, Phys. Rev. **121**, 1090 (1961).

[63] K. G. Wilson, The renormalization group: Critical phenomena and the Kondo problem, Rev. Mod. Phys. **47**, 773 (1975).

[64] R. Bulla, T. A. Costi, and T. Pruschke, Numerical renormalization group method for quantum impurity systems, Rev. Mod. Phys. **80**, 395 (2008).

[65] R. Žitko and T. Pruschke, Energy resolution and discretization artefacts in the numerical renormalization group, Phys. Rev. B **79**, 085106 (2009).

[66] R. Žitko, NRG Ljubljana (Zenodo, 2021), https://doi.org/10.5281/zenodo.4841076.

[67] A. Weichselbaum and J. von Delft, Sum-rule conserving spectral functions from the numerical renormalization group, Phys. Rev. Lett. **99**, 076402 (2007).

[68] D. Goldhaber-Gordon, J. Göres, M. A. Kastner, H. Shtrikman, D. Mahalu, and U. Meirav, From the Kondo regime to the mixed-valence regime in a single-electron transistor, Phys. Rev. Lett. **81**, 5225 (1998).

[69] T. A. Costi, A. C. Hewson, and V. Zlatic, Transport coefficients of the Anderson model via the numerical renormalization group, J. Phys.: Condens. Matter **6**, 2519 (1994).

[70] T. Koch, J. Loos, A. Alvermann, and H. Fehske, Nonequilibrium transport through molecular junctions in the quantum regime, Phys. Rev. B **84**, 125131 (2011).

[71] J. Loos, T. Koch, A. Alvermann, A. R. Bishop, and H. Fehske, Phonon affected transport through molecular quantum dots, J. Phys.: Condens. Matter **21**, 395601 (2009).

[72] M. Hohenadler and W. von der Linden, Lang–Firsov approaches to polaron physics: From variational methods to unbiased quantum Monte Carlo simulations, in *Polarons in Advanced Materials*, edited by A. S. Alexandrov, Springer Series in Materials Science, Vol. 103 (Canopus/Springer Publishing, 2007).

[73] The maximum of this charge excitation is at slightly larger frequencies than $U_{\mathrm{eff}}/2$ due to the peak's asymmetry. This can be observed also in the pure Anderson impurity model, see, e.g., Ref. [83].

[74] This can be seen in the following way: In general, changing the voltage leads to a different Keldysh component of the hybridization function, which then alters G^{R} at the impurity. However, provided the lead in which the chemical potential is changed is weakly coupled, Δ^{K} does not change with ϕ, and consequently, neither does G^{R}. Then the second term in Eq. (46) becomes zero and the first contains only $G_{R}(\omega, \phi = 0)$.

[75] A. Mitra, I. Aleiner, and A. J. Millis, Phonon effects in molecular transistors: Quantal and classical treatment, Phys. Rev. B **69**, 245302 (2004).

[76] R. Leturcq, C. Stampfer, K. Inderbitzin, L. Durrer, C. Hierold, E. Mariani, M. G. Schultz, F. von Oppen, and K. Ensslin, Franck–Condon blockade in suspended carbon nanotube quantum dots, Nat. Phys. **5**, 327 (2009).

[77] S. Ballmann, R. Härtle, P. B. Coto, M. Elbing, M. Mayor, M. R. Bryce, M. Thoss, and H. B. Weber, Experimental evidence for quantum interference and vibrationally induced decoherence in single-molecule junctions, Phys. Rev. Lett. **109**, 056801 (2012).

[78] Z. Ioffe, T. Shamai, A. Ophir, G. Noy, I. Yutsis, K. Kfir, O. Cheshnovsky, and Y. Selzer, Detection of heating in

current-carrying molecular junctions by Raman scattering, Nat. Nanotechnol. **3**, 727 (2008).

[79] S. J. van der Molen and P. Liljeroth, Charge transport through molecular switches, J. Phys.: Condens. Matter **22**, 133001 (2010).

[80] M. Thoss and F. Evers, Perspective: Theory of quantum transport in molecular junctions, J. Chem. Phys. **148**, 030901 (2018).

[81] M. Galperin, A. Nitzan, and M. A. Ratner, The non-linear response of molecular junctions: The polaron model revisited, J. Phys.: Condens. Matter **20**, 374107 (2008).

[82] P. Weinberg, M. Schmitt, and M. Bukov, Computer simulations, http://quspin.github.io/QuSpin/ (2023).

[83] A. Erpenbeck, E. Gull, and G. Cohen, Quantum Monte Carlo method in the steady state, Phys. Rev. Lett. **130**, 186301 (2023).